Journal of Alloys and Compounds 509 (2011) 6705–6710

Contents lists available at ScienceDirect

Journal of Alloys and Compounds

journal homepage: www.elsevier.com/locate/jallcom

Room temperature crystallization kinetics of amorphous Cu_6Sn_5 + C alloys

J.S. Thorne[a], J.R. Dahn[a,b], M.N. Obrovac[c], R.A. Dunlap[a,b,d,*]

[a] Department of Physics and Atmospheric Science, Dalhousie University, Halifax, N.S. B3H 3J5, Canada
[b] Institute for Research in Materials, Dalhousie University, Halifax, N.S. B3H 1Z5, Canada
[c] Department of Chemistry, Dalhousie University, Halifax, N.S. B3H 4J3, Canada
[d] College of Sustainability, Dalhousie University, Halifax, N.S. B3H 1W5, Canada

ARTICLE INFO

Article history:
Received 15 February 2011
Accepted 26 March 2011
Available online 5 April 2011

Keywords:
Cu–Sn alloys
Nanostructured materials
Crystallization
X-ray diffraction
Li-ion battery
Electrode materials

ABSTRACT

Thin film combinatorial sputter deposited Cu_6Sn_5 + C alloys were prepared and found to be amorphous and/or nanostructured upon removal from the sample preparation chamber. Samples having approximate compositions $(Cu_6Sn_5)_{1-x}C_x$ with $0.16 < x < 0.26$ have been stored at room temperature and investigated over the course of about one year using X-ray diffraction (XRD). Simple models were employed to analyze the observed changes in the XRD patterns. Relatively sharp (nanocrystalline) components having Bragg angles corresponding to hexagonal Cu_6Sn_5 grew in intensity at the expense of broader (amorphous) components as a function of time. The grain size of the nanocrystalline components was approximately time independent, but depended on the amount of carbon present. The logarithm of the recrystallization time and the activation energy for crystallization appeared to be linearly dependent on the carbon content for the composition range that has been studied, as inferred from the Avrami–Johnson–Mehl equation. XRD patterns of samples with $x > 0.26$ appear to be relatively unchanged after a period of storage at room temperature for one year.

© 2011 Elsevier B.V. All rights reserved.

1. Introduction

Cu–Sn based materials have been considered as candidates for use as negative electrode materials in Li-ion batteries [1–7]. Work in this area has focused primarily on Cu_6Sn_5 with an effort to create nano-sized Cu–Sn grains to help reduce damaging effects caused by stress/strain due to volume changes upon lithiation [1,8,9]. It is widely believed that amorphous or nanostructured materials are best suited for high-volume expansion alloys such as Sn to further reduce the effects of expansion and contraction [10]. A number of thin film amorphous alloy negative electrode materials for Li-ion batteries have been prepared using combinatorial sputter deposition [9,11–14]. These include amorphous Sn–Co–C and other Sn–TM–C alloys (TM = Ti, V and Cu). The addition of carbon to the Sn–Co system [11] and other Sn–TM systems [13] including the Sn–Cu system [9] is responsible for a marked decrease in grain size and an improvement in cycle life.

Combinatorial sputtering can be used for analyzing samples covering a large range of compositions [13]. The main application of high throughput combinatorial sputtering is composition optimization of systems with two or more elements. However, the stability of such resulting alloys prepared by this method may be a concern and should be considered in a comparison with nanostructured samples prepared by other methods such as mechanical alloying, electroplating or co-precipitation.

Sputter deposited $(Cu_6Sn_5)_{1-x}C_x$ alloys with $x < 0.3$ have been shown to comprise an intimate mixture of Sn, Cu and C nearest neighbors using Sn Mössbauer spectroscopy [9]. During early lithation/delithiation cycles the differential capacity curves of cells utilizing these materials as anodes have been shown to be unstable. This results from the crystallization or agglomeration of small regions of Cu_6Sn_5 during Li insertion and extraction [9]. Our investigations of these materials have suggested that Cu_6Sn_5 agglomeration may also occur over extended periods of time at room temperature in amorphous samples with low carbon content. The present investigation considers the long term stability of the structure of metastable Cu_6Sn_5 + C samples that have previously been reported in electrochemical studies [9]. These studies may have implications for the practical use of these materials, in particular, but also emphasizes the importance of stability considerations for nanostructured materials in general.

Other Cu-based alloys have been found to recrystallize to form larger grains of pure Cu at room temperature [15–18]. Room temperature crystallization of electroplated amorphous Cu at room temperature has been observed with initial thicknesses on the

* Corresponding author at: Department of Physics and Atmospheric Science, Dalhousie University, 6300 Coburg Road, Halifax, N.S. B3H 3J5, Canada.
E-mail addresses: jsthorne@dal.ca (J.S. Thorne), dunlap@fizz.phys.dal.ca (R.A. Dunlap).

0925-8388/$ – see front matter © 2011 Elsevier B.V. All rights reserved.
doi:10.1016/j.jallcom.2011.03.150

order of 3 μm or less [16,17]. This crystallization process has been referred to as "self annealing" [17].

2. Experimental methods

Pseudo-binary libraries in the Sn–Cu–C system were produced using combinatorial sputtering methods similar to those described elsewhere [9,11,19]. Substrates included Si, for X-ray diffraction (XRD), compositional studies and thickness measurements, and Cu (for mass measurements). The sputtering parameters used and the target compositions for the library presented in this work are given in Table 1. The library had a Cu:Sn ratio approximately the same as in Cu_6Sn_5 and a varying C composition. All sputtering targets were 5.08 cm in diameter. The Cu targets were cut from 0.635 cm thick Cu plate (3N purity). Two 0.635 cm thick carbon sputtering targets (5N purity) were obtained from Kurt J. Lesker Co. (Clairton, PA). The 2N85 purity Sn sputtering target was 0.330 cm thick and was cut from a Sn plate obtained from Alfa Aesar (Ward Hill, MA). All targets were mounted on 0.318 cm thick copper backing plates using SilverTech PT-1 silver epoxy from Williams Advanced Materials.

Electron microprobe measurements were made using a JEOL JXA-8200 Superprobe to determine composition as a function of position across the film and to verify that the intended composition range was achieved. The microprobe is equipped with a translation stage which allows the composition measurements to be matched with the results of the XRD measurements.

XRD measurements were performed using an INEL CPS120 curved position-sensitive detector coupled to an X-ray generator equipped with a Cu target X-ray tube. A monochromator in the incident beam path limits the wavelengths striking the sample to Cu-K_α radiation ($\lambda = 1.54$ Å). As the X-ray tube was quite old, the copper target had partially sputtered through to the tungsten support, yielding weak $W_{L\alpha}$ ($\lambda = 1.48$ Å) peaks in the diffraction patterns. These were not considered in the analysis of the patterns and did not affect the results presented here. The incident angle of the beam with respect to the sample is about 6°, which does not satisfy the Bragg condition for the (1 0 0) peaks for the Si wafer used as a substrate allowing for zero-background measurements. The detector measures the entire diffraction pattern between scattering angles of 6° and 120° at once using a 2400 second dwell time. A translation stage allows for diffraction patterns to be obtained as a function of position, and hence composition, on the combinatorial library.

Samples were measured and compared at times of 1 day, 14 days, 40 days, 80 days, 150 days and 350 days after removal from the sputter chamber for two separate films having the same sputter parameters, and hence the same nominal composition range, to ensure validity of the results. In order to confirm that integrated X-ray flux did not have an effect on the sample microstructure, one film was X-rayed six times during one day and no measurable changes were observed in the patterns.

3. Results and discussion

The composition of the present library as obtained from the electron microprobe studies is illustrated in Fig. 1 as a function of position on the film. Measurements of the mass as a function of position together with the bulk densities for Sn, Cu and C, yielded film thickness between 540 and 580 nm. This is in close agreement with measured values of the film thickness as a function of position. Film thickness is a key parameter in the rate of self annealing of thin film amorphous samples [16,17]. Primary sources of error in the stated compositions come from the uncertainty in the position of the measured XRD patterns on the film as a function of time. The uncertainty in measured position is estimated to be ±1 mm and a linear fit of the composition measurements indicates that this corresponds to an uncertainty of about ±1 at.% carbon (i.e. $x \pm 0.01$) in all compositions reported here.

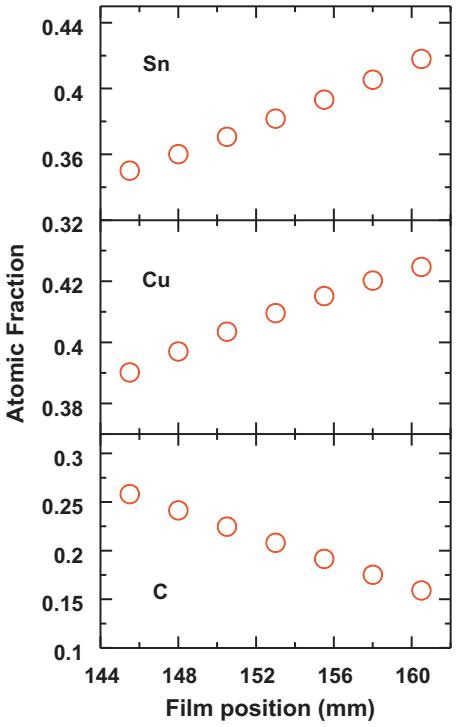

Fig. 1. Atomic fraction of Sn, Cu and C for selected samples analyzed in this work as a function of the film position.

Fig. 2 shows selected XRD patterns of $(Cu_6Sn_5)_{1-x}C_x$ with $0.18 \leq x \leq 0.24$ as a function of time. A single composition is shown in each row of the figure (each within the specified composition uncertainty) with different times shown in each column as indicated. Samples showed atomic agglomeration or crystallization at room temperature as a function of time. Bragg peaks emerged near scattering angles of 30 and 43°, corresponding to the main peaks found in hexagonal Cu_6Sn_5. As the carbon content increased from $x = 0.18$ to $x = 0.24$, however, the crystallization process occurred more slowly. Samples with $x \geq 0.28$ (and with a film thickness near 580 nm) showed no visible changes in the diffraction patterns after 350 days.

The following simple model was utilized to extract a meaningful interpretation of the diffraction patterns observed in Fig. 2. The appearance of the broad amorphous "humps" is assumed to be a result of Sn–Sn nearest neighbour correlations (left hump) and Sn–Cu/Cu–Cu nearest neighbour correlations in the amorphous alloy (right hump) [20]. For patterns which were purely amorphous (i.e. no hexagonal Cu_6Sn_5 Bragg peaks), adequate fits were achieved using two pseudo-Voigt peaks, each given by

$$y = h\left(\frac{s}{1+[2(\theta-\theta_0)/\Gamma]^2} + (1-s)\exp\left[-\frac{2(\ln 2)(\theta-\theta_0)}{\Gamma}\right]\right) \quad (1)$$

where 2θ is the scattering angle, h is the peak area, s is the shape factor ($0 < s < 1$), θ_0 is the center and Γ is the half width at half maximum. All the fitting parameters were free with the exception of the pseudo-Voigt used to fit the Sn–Sn hump, for which the shape factor was fixed to be 1 (thus making it a pure Lorentzian). In addition, a linear function was used to fit the background part of each pattern.

For diffraction patterns which were observed to have sharp (nanocrystalline) components, a second set of peaks were included in the fits. In these cases all pseudo-Voigt fitting parameters for the

Table 1
Target compositions and sputtering parameters used to produce the combinatorial Sn–Cu–C library.

Target composition range	Pressure (mTorr)	Power Sn (W)	Power Cu (W)	Power C (W)
$Sn_xCu_yC_{1-x-y}$ $x/(x+y) = 0.48$ $0 < 1-x-y < 0.45$	2.0	14	9	2×149

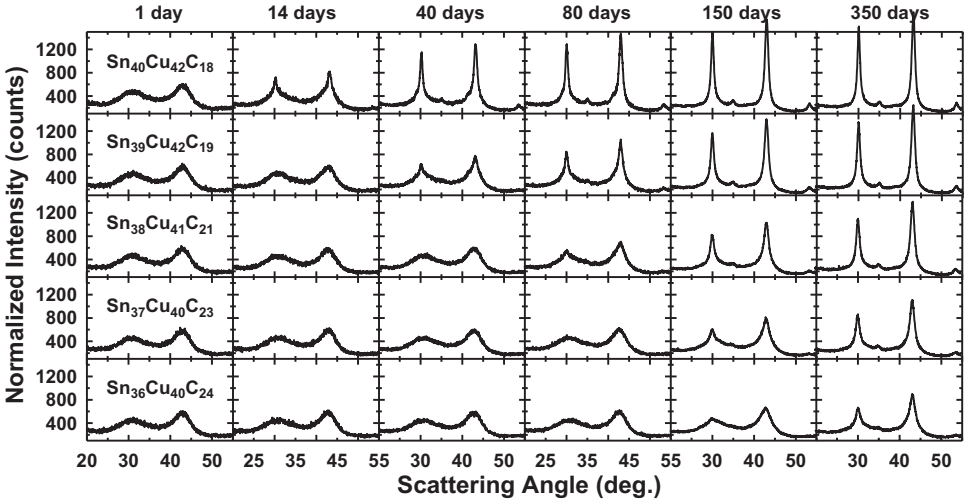

Fig. 2. Time dependence of selected XRD patterns. The approximate composition is indicated and is constant for each row. The time of each measurement is indicated and is constant for each column.

amorphous components were fixed and were then multiplied by a single fitting parameter which was used to scale the total area. Two Lorentzian peaks (i.e. with a shape factor of 1 in Eq. (1)) were used to fit the crystalline components. Fig. 3 shows an illustration of the fitting model for a $Sn_{40}Cu_{42}C_{18}$ sample for the first three measurement times as indicated. The relative area of the nanocrystalline component increased with time.

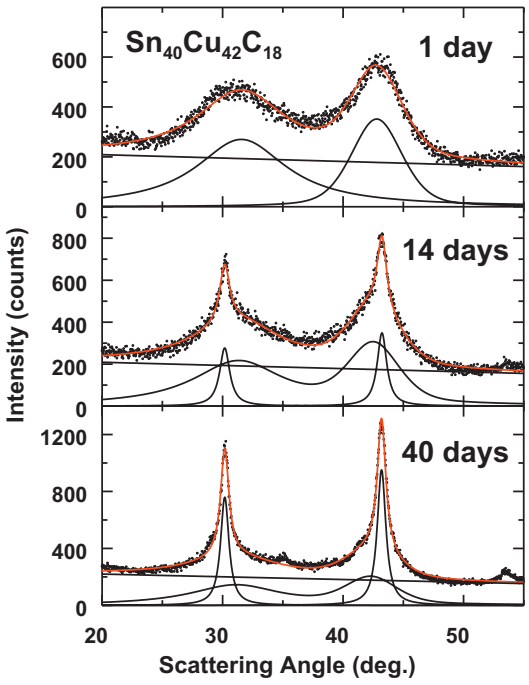

Fig. 3. XRD patterns of a sample having an approximate composition $Sn_{41}Cu_{42}C_{17}$. at selected times. Shown is the raw data, overall fit (red line), and fit components (black lines). Fitting methods are described in the text. (For interpretation of the references to color in this figure legend, the reader is referred to the web version of the article.)

Fig. 4 shows the grain size of the nanocrystalline components as extracted using the Scherrer equation;

$$\tau = \frac{0.9\lambda}{\beta \cos\theta} \tag{2}$$

where λ is the X-ray wavelength (Cu-K_α), θ is the Bragg angle and β is the full width at half maximum (FWHM) in 2θ. A shape factor of 0.9 was used. The amorphous components do not give meaningful results from the Scherrer equation. Fig. 4 shows the average grain size as obtained from Eq. (2) for the nanocrystalline components. The grain size for a given carbon content appears to be virtually independent of time, and hence is independent of the relative amplitude of the nanocrystalline component. This suggests that secondary grain growth is occurring. A similar result has been observed in thin film Cu, as well as Au and Si, where grain aggregation appeared to occur with a bimodal grain size distribution until completion of the transformation [17].

Fig. 5 shows the sum of the areas of the Bragg peaks of the nanocrystalline components divided by the total peak area as a function of time for each sample. The total peak area is simply the sum of the areas of the nanocrystalline components plus the amorphous components and does not include the background. The relative area of the crystalline components increased faster as a function of time for samples with less carbon. As carbon is added, some fits were not improved with the addition of the crystalline components until later times. Adding carbon therefore impedes the crystallization process.

The kinetics of crystallization seen in Fig. 5 are well described by commonly used models for thermally induced reactions. These can be derived from,

$$\frac{dA}{dt} = k(T)f(A) \tag{3}$$

where A is the fraction of sample recrystallized and T is the temperature. Using separation of variables, the reaction model $f(A)$ can be found based on a number of physical situations [21]. In this case, crystallization of thin film Sn–Cu–C was well described by the Avrami–Johnson–Mehl equation, as has been used to help describe

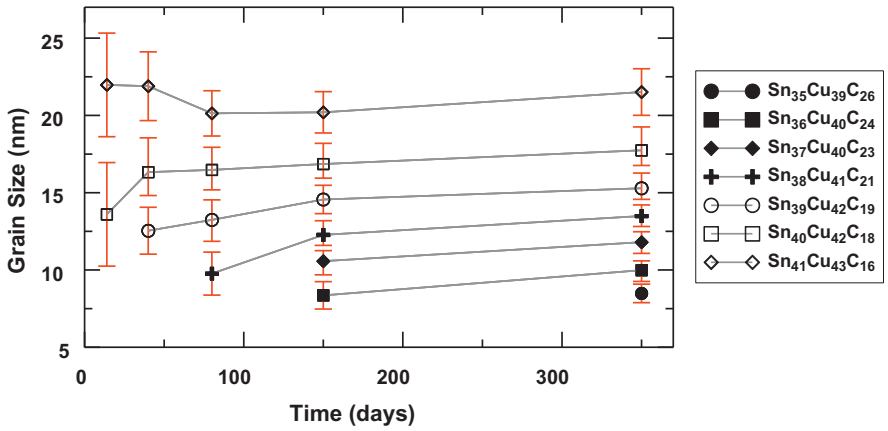

Fig. 4. Time dependence of the grain size as extracted by the Scherrer equation for selected samples. Compositions are indicated.

room temperature crystallization of electroplated Cu trenches [16]. This is given by,

$$A = 1 - e^{-kt^n}. \tag{4}$$

where A is the volume fraction of the crystalline component, k is the rate constant (in units of s^{-n}), and n is the Avrami exponent. This can also be written in the form,

$$A = 1 - e^{-(t/t_R)^n}. \tag{5}$$

where t_R is the time in which $1 - e^{-1} \approx 63\%$ of the sample has recrystallized. It is conceivable that not all of the sample will undergo crystallization, or that the statistics of the XRD patterns in combination with the fitting model used do not adequately reflect the fraction of amorphous sample remaining as the amorphous component becomes small. Therefore, it is assumed that some fraction of the sample is inert during the duration of the experiment and Eq. (4) is obeyed for some fraction A_{max} of the components. Eq. (4) becomes

$$A = A_{max}(1 - e^{-kt^n}) = A_{max}(1 - e^{-(t/t_R)^n}) \tag{6}$$

The three parameter model described by Eq. (6) was used to fit the relative areas found in Fig. 5, and the rate constant (or t_R) was obtained for each sample. The value of A_{max} was fixed at a value of 0.78 for all fits. Eq. (6) can be rearranged to obtain

$$-\ln\left(-\ln\left(\frac{1-A}{A_{max}}\right)\right) = -n\ln(t) + \ln\left(\frac{1}{k}\right) \tag{7}$$

A plot of $-\ln(-\ln(1 - A/A_{max}))$ as a function of $\ln(t)$, also known as an Avrami plot, is expected to be linear with slope $-n$ and y-intercept $\ln(1/k)$. This can be found in Fig. 6 for the extracted values and best fit lines presented in Fig. 5. Values for which $1 - A/A_{max} = 0$ or 1 are not defined on the Avrami plot according to Eq. (7). There is an approximately linear dependence of the available data (within error) and best fit lines are generally within the bounds of the error.

Fig. 7 shows the best fit parameters in Eqs. (6) and (7) for each of the seven samples presented in this work as a function of carbon content. Fig. 7 shows an approximately linear dependence of the Avrami exponent and $\log(t_R)$ as a function of carbon content. The recrystallization time t_R is seen to vary between 22 and 648 days as the carbon content is increased from 0.16 to 0.26. Fig. 7 also shows the linear dependence of the logarithm of the rate constant as a function of carbon content. The rate constant is commonly assumed to be of the Arrhenius form, related to the activation energy by

$$k = k_0 e^{-E_a/k_B T} \tag{8}$$

where k_0 is a constant, E_a is the activation energy, k_B is the Boltzmann constant and T is the temperature [18].

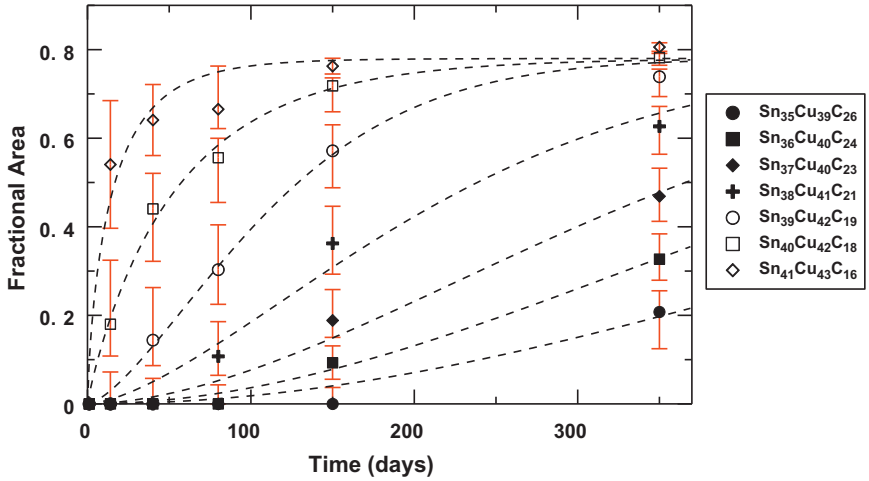

Fig. 5. Time dependence of the relative area of the fitting components for selected samples with compositions indicated. Shown is the area of the nanocrystalline components divided by total area which are assumed to be proportional to the volume of each component present in the sample. The linear background component is not included. Best fit lines according to the Avrami–Johnson–Mehl equation (see Eq. (5)) are included for comparison.

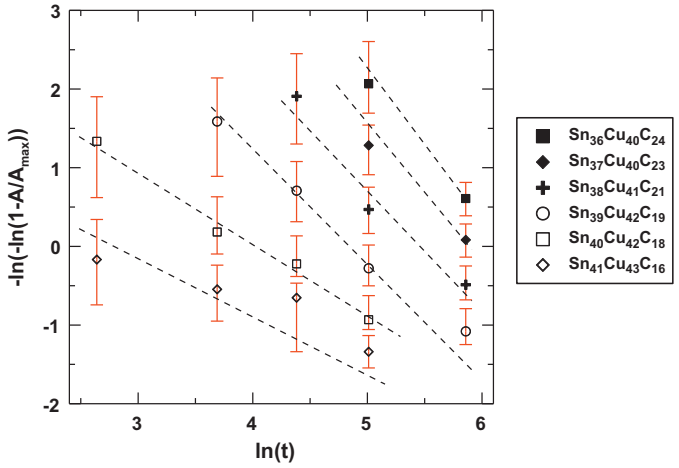

Fig. 6. Avrami plot of the available data with compositions indicated. Best fit lines shown in Fig. 5 are included for comparison. The time is in units of days.

Interpretation of the results presented above is as follows: Sn, Cu and C atoms diffuse, which can result in the formation of small grained regions of Cu_6Sn_5. It may be assumed that carbon is expelled from these regions and forms areas of pure carbon during the formation of the Cu_6Sn_5 grains. As Fig. 4 shows, there also appears to be a limit to the size of the Cu_6Sn_5 grains as determined by carbon content. The increasing value of the Avrami exponent n as carbon is added may be attributed to higher rates of nucleation. However, the increased nucleation also comes at the expense of increased crystallization time (i.e. lower growth rate) as seen in Fig. 7. For constant nucleation rate with decreasing growth rate, values of n are expected to be no less than 1 [22]. Values of n less than 1 are attributed to both a decreasing growth and nucleation rate. This comes as a result of the decreasing concentration gradient of reactant (amorphous Sn + Cu + C) and product (nanostructured Cu_6Sn_5 + C) as the sample is crystallized [22]. This effect may explain anomalously low values of n observed for some samples presented in this work. Since the temperature dependence of the rate constants were not measured, it is not possible to quantify the activation energies due to the unknown frequency factor k_0. However, comparison of the functional form of Eq. (8) with Fig. 7 shows that the activation energy (as inferred by the Avrami–Johnson–Mehl equation) is approximately linearly dependent on the atomic fraction C in thin film amorphous Cu_6Sn_5 + C samples.

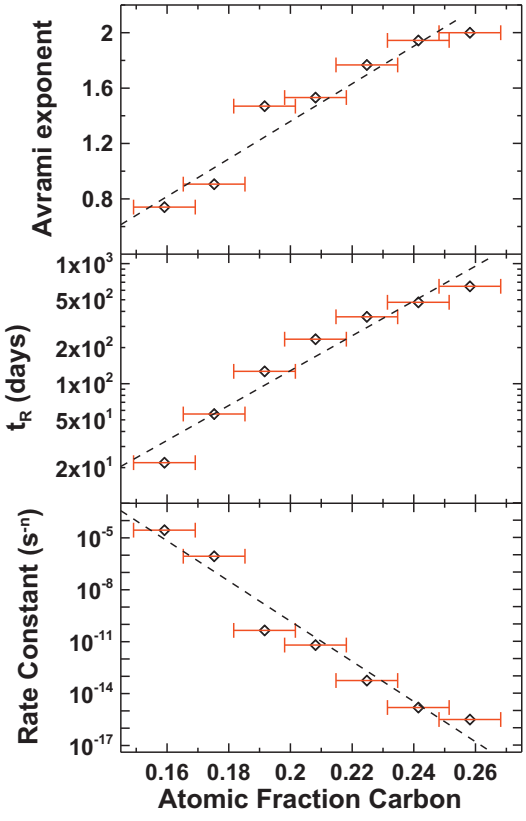

Fig. 7. The Avrami exponent, recrystallization time t_R, and rate constant as a function of carbon content for the film. The recrystallization time and rate constant are plotted on a logarithmic scale.

4. Conclusion

Combinatorial sputtering is a useful method for characterizing samples over a wide range of compositions. However, intimate mixtures of atoms resulting from many layers of monolayer deposition can result in the formation of metastable phases in thin film samples. As has been demonstrated, the structure of these metastable mixtures may change as a function of time even at room temperature.

A simple model was used to characterize the crystallization process. XRD patterns were modeled as a mixture of amorphous regions plus crystalline regions. Using the Scherrer equation it was found that the increasing amplitude of the crystalline regions was associated with an approximately constant grain size. Bimodal grain size distribution has also been observed for the room temperature recrystallization of Cu [17]. Finally, it was inferred that the activation energy is roughly linear as a function of carbon content in the samples studied in the present work. This observation suggests one possible mechanism by which amorphous or nanostructured Sn–TM–C thin films, or other metastable alloys, may crystallize over extended periods of time at room temperature.

Acknowledgements

The authors acknowledge funding from NSERC and 3M Canada, Co. under the auspices of the Industrial Research Chairs Program. We also acknowledge the support of the Canada Foundation for Innovation, the Atlantic Innovation Fund and other partners that fund the Facilities for Materials Characterization managed by the Institute for Research in Materials.

References

[1] K.D. Kepler, J.T. Vaughey, M.M. Thackeray, J. Power Sources 81 (1999) 383.
[2] D. Larcher, L.Y. Beaulieu, D.D. MacNeil, J.R. Dahn, J. Electrochem. Soc. 147 (2000) 1658.
[3] S.D. Beattie, J.R. Dahn, J. Electrochem. Soc. 150 (2003) A894.
[4] J. Wolfenstine, S. Campos, D. Foster, J. Read, W.K. Behl, J. Power Sources 109 (2002) 230.
[5] D.G. Kim, H. Kim, H.J. Sohn, T. Kang, J. Power Sources 104 (2002) 221.
[6] J. Park, J. Eom, H. Kwong, Electrochim. Acta 55 (2010) 1825.
[7] L. Trahey, J.T. Vaughey, H.H. Kung, M.M. Thackeray, J. Electrochem. Soc. 156 (2009) A385.
[8] O. Mao, R.L. Turner, I.A. Courtney, B.D. Fredericksen, M.I. Buckett, L.J. Krause, J.R. Dahn, Electrochem. Solid-State Lett. 2 (1999) 3.
[9] J.S. Thorne, R.J. Sanderson, J.R. Dahn, R.A. Dunlap, J. Electrochem. Soc. 157 (2010) A1085.
[10] W.-J. Zhang, J. Power Sources 196 (2010) 13.
[11] J.R. Dahn, R.E. Mar, A. Alyaa, J. Electrochem. Soc. 153 (2006) A361.
[12] A.D.W. Todd, R.E. Mar, J.R. Dahn, J. Electrochem. Soc. 153 (2006) A1998.
[13] A.D.W. Todd, R.E. Mar, J.R. Dahn, J. Electrochem. Soc. 154 (2007) A597.
[14] A.D.W. Todd, P.P. Ferguson, M.D. Fleischauer, J.R. Dahn, Int. J. Energy Res. 34 (2010) 535.
[15] M. Fukuhara, H. Abe, H. Nishikawa, T. Takemoto, G. Xie, A. Inoue, Chem. Phys. Lett. 469 (2009) 289.
[16] C. Lingk, M.E. Gross, J. Appl. Phys. 84 (1998) 5547.

[17] S.H. Brongersma, E. Richard, I. Vervoort, H. Bender, W. Vandervorst, S. Lagrange,.G. Beyer, K. Maex, J. Appl. Phys. 86 (1999) 3642.
[18] T. Zhaosheng, B. Zhang, H. Zhang, J. Mater. Sci. 27 (1992) 4021.
[19] J.R. Dahn, S. Trussler, T.D. Hatchard, A. Bonakdarpour, J.N. Meuller-Neuhaus, K.C. Hewitt, M. Fleischauer, Chem. Mater. 14 (2002) 3519.
[20] J.F. Geny, G. Marchal, P. Mangin, C. Janot, M. Piecuch, Phys. Rev. B 25 (1982) 7449.
[21] W.E. Brown, D. Dollimore, A.K. Galwey, Compr. Chem. Kinet. 22 (1980) 91.
[22] T. Pradell, D. Crespo, N. Clavaguera, M.T. Clavaguera-Mora, J. Phys. Condens. Matter 10 (1998) 3833.